Structure–Property Relationships in Biomedical Thermoplastic Polyurethane Nanocomposites

ARTICLE *in* MACROMOLECULES · DECEMBER 2012

Impact Factor: 5.8 · DOI: 10.1021/ma202189e

8 AUTHORS, INCLUDING:

Azlin Fazlina Osman
Universiti Malaysia Perlis
34 PUBLICATIONS **62** CITATIONS
SEE PROFILE

Grant Edwards
University of Queensland
28 PUBLICATIONS **98** CITATIONS
SEE PROFILE

Isabel C Morrow
University of Queensland
15 PUBLICATIONS **1,287** CITATIONS
SEE PROFILE

Peter J. Halley
University of Queensland
254 PUBLICATIONS **3,340** CITATIONS
SEE PROFILE

Macromolecules

Article

pubs.acs.org/Macromolecules

Structure–Property Relationships in Biomedical Thermoplastic Polyurethane Nanocomposites

Azlin F. Osman,[†] Grant A. Edwards,[†] Tara L. Schiller,[⊥] Yosephine Andriani,[†] Kevin S. Jack,[†] Isabel C. Morrow,[‡,§] Peter J. Halley,[†] and Darren J. Martin*[,†]

[†]Australian Institute for Bioengineering and Nanotechnology, The University of Queensland, Building 75, Cnr College and Cooper Rds, Brisbane 4072, Australia

[‡]ARC Centre of Excellence for Functional Nanomaterials, The University of Queensland, Australia

[§]Australian Microscopy and Microanalysis Research Facility, The University of Queensland, Australia

[⊥]Department of Materials Engineering, Monash University, Clayton 3800, Australia

ABSTRACT: Polyurethanes are excellent potential materials for the construction of implantable medical components due to their exceptional mechanical properties and biocompatibility. Currently, soft silicone materials are employed as insulation for implantable cochlear electrode arrays. Siloxane-based thermoplastic polyurethane (TPU) nanocomposites containing synthetic layered silicates are being investigated as new insulation materials with superior tensile and tear strength and reduced surface tack, potentially allowing for thinner insulation and more intricate electrode designs. In this work, ElastEon E5-325 (Aortech Pty Ltd.) TPU nanocomposites reinforced with 2 and 4 wt % low aspect ratio organo-hectorite and high aspect ratio organo-fluoromica (Lucentite SWN, Somasif ME100, both modified with octadecyltrimethylammonium (ODTMA)) were prepared by a solvent casting technique. The mechanical properties of the resulting nanocomposites were measured by tensile, tear, stress relaxation, and creep testing and morphologically were characterized by DSC, DMTA, XRD, TEM, and strained *in situ* synchrotron SAXS. We found that the hydrophobic low aspect ratio organohectorite acts as a very potent interfacial compatibilizer. At 2 wt % loading, the resulting nanocomposite displays vastly superior mechanical properties to both soft silicone and ElastEon. In addition to providing 30 nm × 1 nm synthetic nanosilicate reinforcing elements which are readily capable of orientation and reinforcement, these nanosilicates also serve to provide more cohesive hard microdomains and thus creep resistance and dimensional stability. Interestingly, at a higher (4 wt %) loading of organohectorite, gross morphological changes in the TPU microdomain texture are observed, adversely effecting the mechanical properties of the TPU.

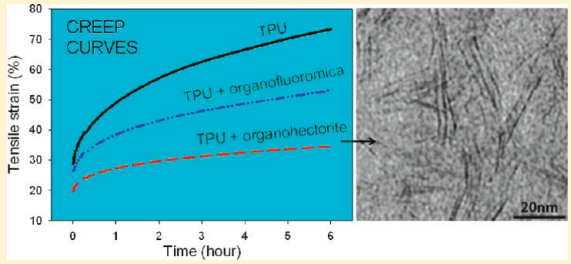

INTRODUCTION

The addition of nanoscale inorganic particles into bulk polymers in order to generate nanocomposites with improved mechanical and chemical properties relative to the parent materials is a rapidly expanding field. The limitless scope for nanofiller materials chemistry and surface chemistry is enabling researchers expanded freedom to bestow further desirable properties on the resulting nanocomposites, thereby enabling the production of novel materials with numerous potential applications. Thermoplastic polyurethane (TPU) is the material of choice for many biomedical applications due to the relative ease of fabrication into devices, flexibility, biocompatibility, biostability, and electrical insulation properties. Polyether-based TPUs have been the materials of choice for certain types of medical implants for many years.[1,2] However, there were some cases where the TPU degraded and led to surface or deep cracking, stiffening, erosion, or the deterioration of mechanical properties such as tensile and flexural strength.[3−7] These inherent deficiencies in the material eventually caused implant malfunction. Poly(dimethylsiloxane) (PDMS)-based TPU were then commercialized and introduced to overcome these problems. The PDMS/poly(hexamethylene oxide) (PHMO)-based TPU based on an optimized formulation (Elast-Eon) from AorTech Biomaterials Pty Ltd. exhibits properties comparable to those of medical grade polyether-based TPU materials such as Pellethane 80A.[8] Elast-Eon TPU are now widely accepted as being the most biostable of all the TPUs and as such are imminently suitable for long-term implantation.[9]

Use of TPU as the nanocomposite matrix presents some interesting challenges to the understanding of the nanoscale and microscale morphology due to the preexisting morphology of the segmented TPU domains (the so-called phase-separated soft and hard segment rich phases). Knowledge in the TPU nanocomposite area has progressed recently, with several research papers discussing the effects of nanofillers on TPU morphology, highlighting the importance of understanding the

Received: September 29, 2011
Revised: December 2, 2011
Published: December 12, 2011

specific hard segment and soft segment interactions with the nanofillers in correlation with the resulting nanocomposite properties. As reported by Mishra et al.,[10,11] Korley et al.,[12] Kim et al.,[13] and Barick et al.,[14] the surface modifier hydrophobicity can affect the degree of interaction between the nanosilicate and the TPU segments, and thus their dispersion in the matrix, and consequently determines the mechanical behavior of the resulting nanocomposites. In more recent work, Smart et al.[15] demonstrated that the degree of TPU hard and soft segments−nanofiller interactions in a TPU-functionalized carbon nanotube system depended on the functional group alkyl tail lengths, and this strongly influenced the nanofiller dispersion in the TPU and tensile properties of the nanocomposite. These findings show that there is a possibility to control the degree of specific segmental interactions with particular nanofiller in the TPU matrices by exploiting the molecular interactions. If we understand and control these molecular interactions, then we have an opportunity to target and improve specific macroscopic properties of the TPU nanocomposites.

In an attempt to produce new biomaterials with improved properties for the insulation of cochlear electrode arrays, we have recently generated ElastEon E5-325 TPU nanocomposites containing high and low aspect ratio organosilicates with a hydrophobic surface modification. Here we describe the complete mechanical and morphological characterization of the E5-325 TPU and associated nanocomposites in attempt to develop an in-depth understanding of structure−property relationships of these materials, most importantly the interplay between TPU nanophase domains with engineered low and high aspect ratio nanofillers. To the best of our knowledge, this is the first time the structure−property relationships of the PDMS-based TPU nanocomposites have been thoroughly studied. The interactions of these organically modified layered silicate nanofillers in concert with a TPU host polymer incorporating such a hydrophobic soft segment has provided us with new and interesting ways to perturb biomedical TPU property profiles.

EXPERIMENTAL SECTION

Materials. Nusil MED 4860 is a medical grade elastomer with two-part silicone system in 1:1 mix ratio (part A:B). Part A consists of 30 wt % amorphous silica, while part B includes an additional 5 wt % dimethyl, methylhydrogen siloxane copolymer. Once these two parts mixed, Nusil MED 4860 undergoes rapid curing at 165 °C for 5 min due to the presence of platinum. This material was supplied by Cochlear Ltd. and is commercially available from Nusil (via EIM distributors in Australia).

ElastEon E5-325 TPU consists of a 1000 g/mol poly(dimethylsiloxane) (PDMS) and 700 g/mol poly(hexamethylene oxide) (PHMO) mixed soft segment in a 98:2 (w/w) ratio and a hard segment composed of alternating 4,4′-methylene diphenyl diisocyanate (MDI) and 1,4-butanediol (BDO) sequences. The hard segment concentrations is 32.5 wt %. This TPU was supplied by AorTech Biomaterials Pty Ltd. Hectorite (Lucentite SWN) is a synthetic trioctahedral smectite and was used as-supplied from the Kobo Products, Inc. It is a white powder with the chemical formula $Na_{0.66}[Si_8(Mg_{5.34}Li_{0.66})O_{20}(OH)_4]^{-0.66}$ and an average particle diameter size of approximately 30−50 nm. Fluoromica (Somasif ME100), which is a synthetic mica (tetrasilicic trioctahedral fluoromica), was supplied by Kobo Products, Inc. It is a white fine powder having an average platelet size of ∼650 nm[16] with the chemical formula $Na_{0.66}Mg_{2.68}(Si_{3.98}Al_{0.02})O_{10.02}F_{1.96}$. This comparison of nanosilicate aspect ratio is an important part of this study. The surface modification of the nanosilicate was performed by exchanging with octadecyltrimethylammonium (bromide) (ODTMA) using a previously published method.[16,17]

Sample Preparation. E5-325 TPU nanocomposites with two different types of ODTMA-modified nanosilicates; ME100 (ME) and Lucentite (Lu) were prepared in 2 and 4 wt % compositions. These organosilicates were prepared as 5 wt % solution in toluene, while the TPU was prepared as 5 wt % solution in dimethylacetamide (DMAc). To ensure dispersion, the organosilicate was placed in a small glass bottle and was then placed in an ultrasonic bath for ∼1 h. The sample was then dispersed further by a high-energy ultrasonic probe for 2 min of exposure and then followed by another hour of dispersion in the ultrasonic bath. These steps were done to ensure a high level of swelling in the nanoclays before homogenizing. The dispersed organosilicate was added to solution of TPU in DMAc. This was done to give a final composition of 2 and 4 wt % of nanofiller loading in the TPU. The combined solution was then mixed vigorously for 1 min in a high-shear homogenizer, followed by stirring overnight at room temperature with a magnetic stirrer. The solution was then poured into a glass mold. The films were dried at 60 °C for ∼72 h under a nitrogen purge. It is important to ensure that the films are free of moisture. If moisture is not carefully excluded during casting, this can result in low-quality cloudy films with inferior properties. The solvent-cast films were then annealed under vacuum at 85 °C for ∼5 h and left to age for at least a week prior to testing. In subsequent discussion, these nanocomposites are referred to as 2MEO, 4MEO, 2LuO, and 4LuO. A number denotes the nanosilicate wt % loading (2 or 4) in the TPU. The first two letters represent type of nanosilicate used (ME = ME100, Lu = lucentite), and the last letter (O) represents the ODMTA modification.

Mechanical Testing. All mechanical tests were carried out at room temperature on an Instron model 5543 universal testing machine with a capacity of 500 N load cell. Five (5) and three (3) replicates of each material were used for tensile and tear tests, respectively. For the tensile tests, dumbbells were punched from an ASTM D-638-M-3 die and a crosshead speed of 50 mm/min was applied. Stress relaxation tests were performed by stretching the specimens to the desired strain (50%) and recording stress vs time data for 10 times the time taken to reach the desired strains. The creep test was conducted according to ISO 899-1:2003, with a stress of 2 MPa and 6 h holding time. Tear strength was measured according to the ISO 34-1:1994 Method B(a), using angle test specimen (type B) without nick, with a crosshead speed of 500 mm/min. For all tests, pneumatic grips were used to prevent specimen slippage.

Transmission Electron Microscopy (TEM). Thin sections of ∼80 nm thickness were cut using a Diatome diamond knife on a Leica Ultracut UC6FCS cryogenic ultramicrotome at temperatures between −80 and −110 °C to ensure the polymers were in a glassy state. Sections were picked up using 2.3 M sucrose and mounted on 200 mesh copper grids (ProSciTech, Australia). Deionized/Milli-Q/tap water was washed over the grids five times. The grids were then allowed to air-dry in self-closing forceps prior to viewing. Samples were examined at low magnification (12000×) on a JEOL 1011 TEM, Japan, at 100 kV, and images were captured on a SIS Morada 4K CCD camera system. Samples examined at higher magnifications (23000×−93000×) were examined on a Technai F30 FEG TEM (FEI Co., Eindhoven, The Netherlands) operating at 300 kV, and images were captured with a Direct Electron LC1100 lens-coupled 4k × 4k CCD camera system.

X-ray Diffraction (XRD). XRD measurements were conducted on a Bruker D8 Advance X-ray diffractometer with a 0.2 mm slit, using Cu Kα radiation generated at 40 kV and 30 mA. Samples were scanned over a range of $2\theta = 0.5°-10°$ using an increment of 0.02 and a scan speed of 1 s. Samples were mounted on a low background holder and fixed with tape to ensure the surface was flat.

Dynamic Mechanical Thermal Analysis (DMTA). Dynamic mechanical measurements were made using a Rheometric Scientific dynamic thermal mechanical analyzer (DMTA IV) equipped with tensile head and reducing force option. Analysis was performed at 0.1% strain in tension mode using a frequency of 2 Hz and a heating

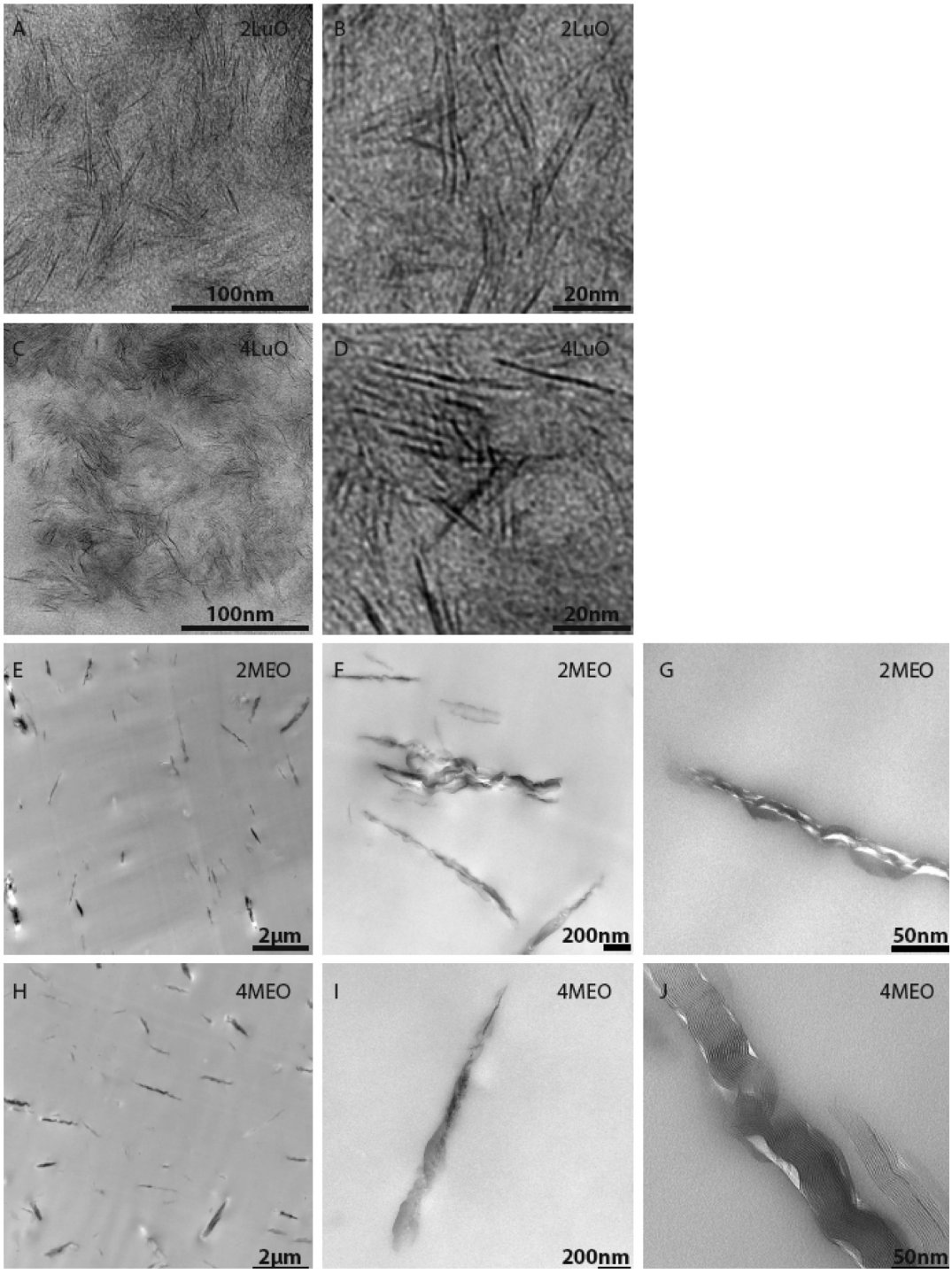

Figure 1. TEM micrographs of 2LuO (A, B), 4LuO (C, D), 2MEO (E–G), and 4MEO (H–J).

rate of 2 °C/min from −100 to 110 °C. We determined that this strain allowed measurements to be taken in the linear viscoelastic regime.

Differential Scanning Calorimetry (DSC). DSC measurements on the TPU and TPU nanocomposites were carried out using the Mettler Toledo DSC 1 Star. The sample weight was ∼6 mg, and the heating rate employed was 10 °C/min. The temperature applied was started from 25 to 250 °C and then cooled to 25 °C at the same ramping rate.

Small-Angle X-ray Scattering (SAXS). *In situ* tensile deformation studies using small-angle scattering (SAXS) technique were carried out on the SAXS/WAXS beamline at the Australian Synchrotron, Melbourne, to obtain morphological information during deformation of TPUs in real time. Two sample-to-detector distances of 0.96 m (short) and 7.2 m (long) were used to measure scattering vector (q) ranges of 0.002–0.06 and 0.015–0.50 Å, respectively. The wavelength of the X-ray beam was 1.240 Å (12 keV). Samples were cut with a dumbbell die with a width of ∼2.5 mm and 15 mm gauge length and strained at a rate of 15 mm/min. Measurements were collected at 0%, 50%, 100%, 200%, 400%, 600%, and 800% strain. For SAXS analysis of the TPU under relaxation, the samples were left to relax after straining for 10 min before collecting a SAXS pattern. The SAXS images were taken immediately after the desired values were reached during either the deformation or the relaxation process. Data acquisition times of 1 and 2 s were used for each measurement at the short and long sample-to-detector distance, respectively.

dx.doi.org/10.1021/ma202189e | *Macromolecules* 2012, 45, 198–210

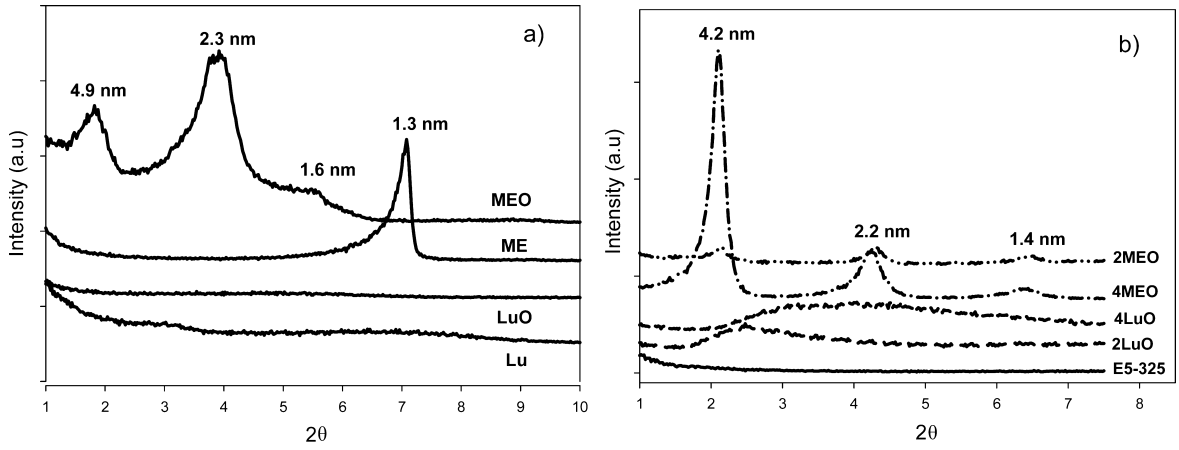

Figure 2. XRD pattern of the (a) pristine ME and Lu nanosilicates and after ODTMA modification (b) the E5-325 TPU containing 2 and 4 wt % MEO and LuO.

Scattering Analysis. Data were analyzed using SAXS15ID version 3299, a program developed at ChemMat CARS as the user interface and control program. The intensity was normalized by the intensity measured at the beamstop to account for changes in transmission due to changes in sample thickness with strain and then further corrected for background scattering. SAXS data averaged over 10° segments in the strain and transverse directions was analyzed using Zernike Prins (ZP) model, which was previously used by Laity et al.[18] and Finnigan et al.[19] to successfully fit SAXS data from TPUs subjected to uniaxial deformation. Based on ZP model, the scattering from two-phase systems can be represented as the product of the form factor, $P(q)$, and the structure factor, $S(q)$:[18−20]

$$I(q) = AP(q)S(q) \tag{1}$$

where q is the scattering vector and A consists of both instrument- and sample-dependent terms and can be treated as a scaling factor. $P(q)$ describes the interference effects between X-rays scattered by different parts of the same scattering body (microdomain) and is dependent upon both the size and shape of the scattering body.[20] The form factor of a sphere of radius (R) is given by

$$P(q) = \left\{3\frac{\sin(qR) - qR\cos(qR)}{(qR)^3}\right\}^2 \tag{2}$$

$S(q)$ represents the interference effects between X-rays scattered by different scattering bodies in the sample and depends on their relative positions and can be described by[18,20]

$$S(q) = \frac{1 - A^2}{1 - 2A\cos(qd) + A^2} \tag{3}$$

where

$$A = \exp\left\{-\frac{q^2\sigma^2}{2}\right\} \tag{4}$$

for the case of a Gaussian distribution of nearest-neighbor distances (d) on the lattice, with standard deviation σ.[18]

The Herman orientation function (f) was used to assess the orientation of both high and low aspect ratio organo-silicates in TPU during tensile deformation and is given by the following equation:[21,22]

$$f = \frac{\langle\cos^2\Phi\rangle - 1}{2} \tag{5}$$

where

$$\langle\cos^2\Phi\rangle = \frac{\int_0^{\pi/2} I(\Phi)\sin\Phi\cos^2\Phi\,d\Phi}{\int_0^{\pi/2} I(\Phi)\sin\Phi\,d\Phi} \tag{6}$$

In this case, f was calculated from the azimuthally averaged data, where $\langle\cos^2\Phi\rangle$ is the average cosine squared weighted by intensity I as a function of the radial angle, Φ. The value of f is equal to 1 and −0.5 when the orientation of the organo-silicate is completely aligned perpendicular and parallel to the direction of strain, respectively, and is zero for random (isotropically) orientated organo-silicates.

RESULTS AND DISCUSSION

Nano-silicate, Organo-silicate, and Nanocomposites Structure. TEM images of the nanocomposites containing ODTMA modified ME (MEO) and ODTMA modified Lu (LuO) are displayed in Figure 1. In general, the low aspect ratio LuO in 2 wt % (2LuO) and 4 wt % (4LuO) dispersed and exfoliated well in the TPU matrix, which is probably due to the hydrophobic ODTMA surfactant providing a favorable thermodynamic driving force for TPU intercalation. The 2LuO system provides 30 nm × 1 nm synthetic clay reinforcing elements which are readily capable of orientation and reinforcement in the TPU. In contrast, 2MEO and 4MEO exhibited an ordered intercalated structure that also contained larger organo-silicate tactoids (in the order of several micrometers) dispersed throughout the TPU matrix. The high aspect ratio MEO with lower mobility and higher spatial restrictions is believed to experience frustrated orientational freedom in the matrix, thus making it more difficult for the intercalated TPU to peel the platelets away from the well-intercalated tactoids.

The XRD signature of any polymer−silicate nanocomposite may be influenced by the average platelet size, degree of nanosilicate interplatelet registration, orientation, and increase in basal spacing (d-spacing) of the nanosilicate due to intercalation by host polymer. The increase in d-spacing depends on the amount of TPU intercalated in the galleries of the silicates,[23−26] and of course, this is a function of nanosilicate loading and also nanocomposite processing history. XRD patterns of the nano-silicates (ME and Lu) and their corresponding organo-silicates, MEO and LuO are shown in Figure 2a, and XRD patterns for their respective nano-composites are shown in Figure 2b. The modification of ME

dx.doi.org/10.1021/ma202189e | Macromolecules 2012, 45, 198−210

Table 1. Mechanical Properties of E5-325 (Neat Host TPU and Nanocomposite) and Nusil MED4860

material	tensile strength (MPa)	Young's modulus (MPa)	elongation at break (%)	toughness (MPa)	tear strength (MPa)
Nusil MED 4860	7.5 ± 0.1	2.7 ± 0.2	595 ± 39	35 ± 4	41 ± 14
E5-325	20 ± 2	10 ± 2	883 ± 63	91 ± 20	53 ± 3
2LuO	23 ± 2	14.4 ± 0.4	1053 ± 60	137 ± 16	70 ± 9
4LuO	10 ± 4	52 ± 12	177 ± 15	15 ± 2	45 ± 1
2MEO	24 ± 1	14.5 ± 0.7	1003 ± 38	131 ± 9	64 ± 1
4MEO	20.2 ± 0.9	11.9 ± 0.3	903 ± 83	105 ± 16	60 ± 5

with ODTMA was observed to substantially increase the (d_{100}) basal spacing from 1.3 to 4.9 nm. However, MEO exhibited several well-defined diffraction peaks as compared to the pristine ME, corresponding to *d*-spacings of approximately 4.9, 2.3, and 1.6 nm, respectively. The additional observed peaks are caused by the interstratified superstructure of the fluoromica, which originates from an inherent heterogeneity.[27,28] This charge heterogeneity may allow different amounts of surfactant chains to intercalate the fluoromica layers, and hence monolayer−bilayer or bilayer−pseudotriple layer arrangements are all possible.[28] The high aspect ratio fluoromica can give rise to long-range order in the resulting organosilicate tactoids (with respect to synthetic hectorites or natural nanosilicates, for example), and this gives rise to strong diffraction peaks. Lu and LuO, in contrast, demonstrate a weak and diffuse diffraction shoulder. One reason for the lack of a strong diffraction peak and the appearance of this diffuse shoulder is that the small aspect ratio of the Lu and LuO may not allow sufficient intensity of the diffraction to be measured due to a reduction in length and ordering of the repetitive layer structure. Existing papers such as those by Finnigan et al.[19] have quantified this effect for TPU systems. This makes interpretation of XRD patterns from LuO-based TPU nanocomposites more difficult, but useful supplementary information can be gleaned. The XRD profile of the neat host TPU shows no significant peak. This is expected, as both soft and hard domains present within a PDMS-based TPU do not show any diffraction peaks between 2θ = 0.5° and 10°,[29,30] and this TPU segmental microphase periodicity can only be detected at lower angles. 2MEO and 4MEO nanocomposites exhibited three well-defined diffraction peaks centered at 2θ = 2.1°, 2θ = 4.2°, and 2θ = 6.4°, corresponding to *d*-spacings of approximately 4.2, 2.2, and 1.4 nm. The small differences in *d*-spacing between the pristine organosilicate and the nanocomposites suggest that there are some large tactoids present where very little, if any, polymer has intercalated into the interlayer spacing. 2LuO, in contrast, demonstrates a weaker and broader peak centered at (d_{001}) of ~2.5°, which corresponds to a *d*-spacing of 3.6 nm. There is also a disruption in the ordering of the organo-silicate platelets when 4LuO is dispersed in the E5-325 TPU matrix. It displays a broad and diffuse diffraction shoulder.

Mechanical Properties. The mechanical properties of solvent cast E5-325 (neat host TPU and nanocomposites) and Nusil MED 4860, a biomaterial that is currently used for insulation in cochlear implants, are summarized in Table 1. The low strain behavior and representative stress−strain curves are shown in Figure 3.

The tensile curve of the neat host E5-325 TPU is similar to that of other TPUs.[26,31,32] E5-325 TPU displays greater tensile properties when compared with Nusil MED4860, showing gains of 167% in tensile strength, 48% in elongation at break, 160% in toughness, and 29% increase in tear strength. Adding 2 wt % of modified organo-silicates further increases the

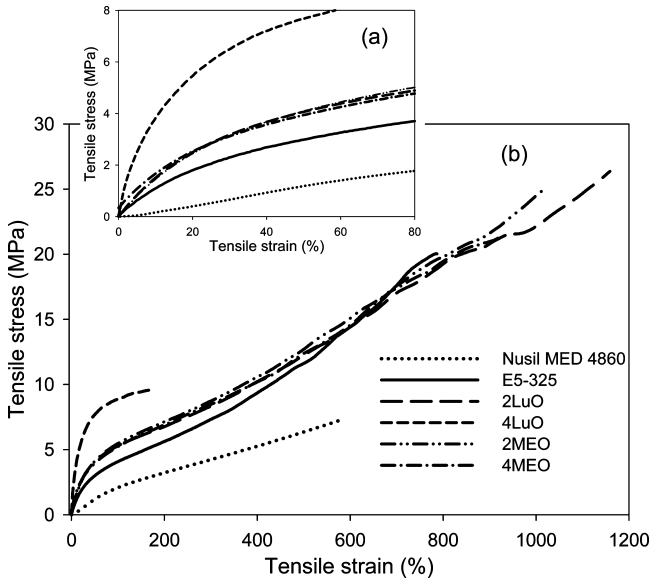

Figure 3. (a) Low strain behavior and (b) stress−strain curves of Nusil MED 4860 and E5-325 (neat host TPU and nanocomposites).

mechanical properties of this PDMS-based TPU. The best mechanical properties were achieved when 2 wt % LuO was added, giving rise to an increase of 15% in tensile strength, 19% in elongation at break, 51% in toughness, and 32% increase in tear strength. We believe that the superior dispersion and delamination of LuO in the TPU matrix (Figure 1) resulted in greater nanofiller−matrix interactions. It has been suggested by Wang and Pinnavaia[33] that the enhancement in tensile strength of elastomeric polyurethane is directly attributed to the reinforcement provided by the dispersed silicate nanolayers. The improvement in extensibility maybe attributed to the plasticizing effect of onium ions, which effects the conformation of the TPU chains at the nanosilicate−matrix interface.[33] These ions would promote relaxation at local stress regions, allowing the material to achieve a higher elongation at the break.[33] However, anomalous behavior was observed when the nanocomposite was prepared at 4 wt % LuO. The addition of this low aspect ratio and hydrophobic organo-silicate resulted in a drastic increase in Young's modulus, and this was accompanied by a large reduction in tensile strength and elongation at break. The Young's modulus was substantially increased by ~420% while the elongation at break was significantly reduced by ~80%. When introduced at 4 wt % loading, the LuO caused a strong perturbation of the TPU morphology. One hypothesis is that the LuO organo-silicate acts as a very potent compatibilizer between the hard segments and soft segments, thereby altering the underlying TPU morphology. The incorporation of 2 wt % modified ME resulted in a slight increase in tensile strength and modulus, with a modest increase in elongation at break as compared to

dx.doi.org/10.1021/ma202189e | Macromolecules 2012, 45, 198−210

the neat host TPU. However, increasing the organo-silicate loading from 2 to 4 wt % resulted in the reduction of both tensile strength and elongation at break, which suggests that there was reduced quality of organo-silicate dispersion compared to the 2 wt % counterpart. The TEM image of 4MEO (Figure 1J) indicates that this material contains larger tactoids than that of 2MEO.

We have also performed the stress relaxation and tensile creep analysis of selected samples to measure their time-dependent dimensional stability under tensile deformation. Stress relaxation data obtained at 50% strain are presented in Figure 4. The data were normalized against the stress, $\sigma(t')$, at t

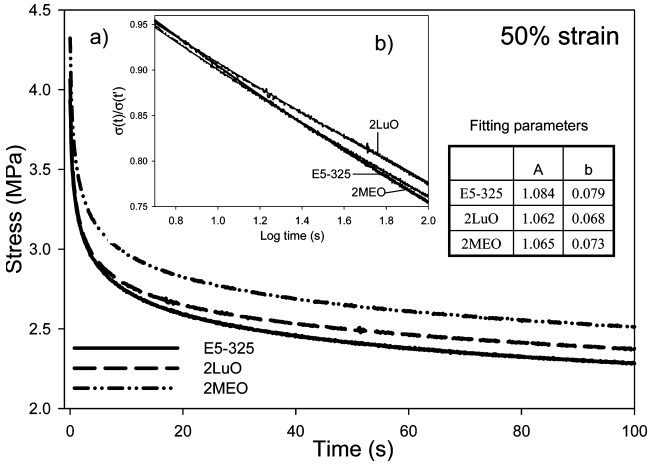

Figure 4. Stress relaxation data obtained at 50% strain.

= 5 s and demonstrated a power-law dependence ($\sigma(t)/\sigma(t') = At^{-b}$), as displayed in Figure 4b. The fitting constants, A and b, from the power law analysis are provided in the inserted table in Figure 4. The slopes of the curves reveal that the stress relaxation rate is reduced with the addition of 2LuO, while the rate is almost unchanged with the 2MEO inclusion. This clearly shows that the low aspect ratio organo-silicate (LuO) was most effective at retarding stress relaxation. According to Sternstein and Zhu,[34] at low strain, the stress relaxation rate in the nanocomposites is considered to be the result of strain-induced disentanglements and slippage of chain segments at the filler surface. Therefore, the low aspect ratio and better dispersed LuO are somehow contributing to reduced strain-induced molecular or segmental slippage and hence a lower stress relaxation rate. The tensile-creep modulus (E_t) (the ratio of applied stress to tensile-creep strain) was used to evaluate the creep resistance of the TPU and the nanocomposites. E_t values for neat E5-325 TPU, 2LuO, and 2MEO measured at a stress of 2 MPa are shown in Table 2, while their representative tensile-

Table 2. Tensile-Creep Modulus (E_t) of the E5-325 (Neat Host TPU and Nanocomposites) Measured at a Stress of 2 MPa

material	tensile creep modulus (MPa)
E5-325	4 ± 1
2LuO	8 ± 1
2MEO	5.3 ± 0.4

creep curves are displayed in Figure 5. The results indicate that the creep resistance of the E5-325 TPU was markedly improved

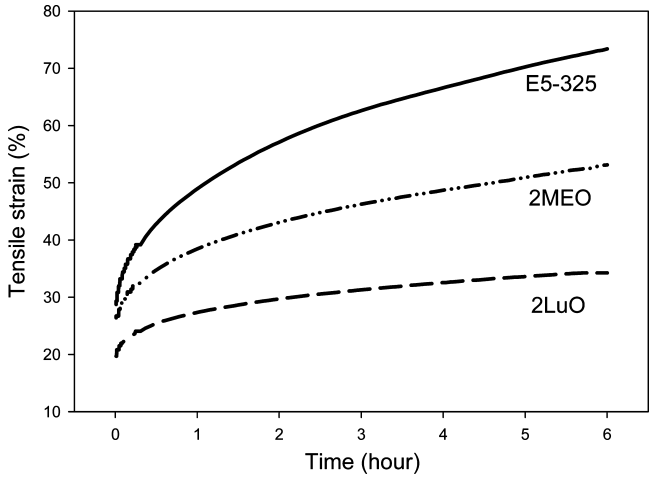

Figure 5. Tensile-creep curves of E5-325, 2LuO, and 2MEO at an applied stress of 2 MPa.

with the addition of 2 wt % LuO and MEO. The highest E_t was achieved by 2LuO with an increase of 100%, while 2MEO resulted in an increase of 26%. This proves that both organosilicates are capable of increasing the creep resistance and dimensional stability of the TPU, in agreement with the stress relaxation study. For an in-depth look into possible reasons for these changes in TPU mechanical behavior with the organo-silicate addition, we performed the DMTA, DSC, and strained synchrotron SAXS analysis to provide information with respect to possible morphological changes and specific TPU–nanofiller molecular interactions.

Dynamic Thermal Mechanical Analysis (DMTA). Tan δ plots in Figure 6a revealed two main peaks for the neat host E5-325, similar to that previously reported by Runt et al.[29,30] on ElastEon TPU with 98% α,ω-PDMS and 2% PHMO and 40% hard segment, where Tα_1 and Tα_2 were observable at −105 and 2 °C, respectively. The first peak corresponds to a low-temperature process (Tα_1), which relates to segmental motion in the PDMS phase.[30] The second peak appears at higher temperature (Tα_2), and this is assigned to the α,ω-PDMS end-group (soft microphase) segmental motion.[29,30]

In our case, Tα_1 is observed in the −84 to −86 °C range, whereas Tα_2 is observed in the 3 to 18 °C range. The Tα_2 of the TPU increased with the addition of the organo-silicates, and this shift was more pronounced in the LuO nanocomposites. The addition of 2 wt % LuO to the E5-325 resulted in an increase of Tα_2 from −3.0 to 7.1 °C while the addition of 4 wt % LuO has significantly increased the Tα_2 from −3.0 to 18.0 °C. In fact, this 4LuO sample exhibits unusual dynamic mechanical properties compared with the neat TPU and its 2 wt % counterpart. It displays a much higher Tα_2 and damping capacity in the rubbery region but lower damping capacity in the glassy region. It is probable that there is phase mixing between the hard and soft segments due to compatibilization of soft and hard segments by this particular organosilicate, so that the Tα_2 of the soft segment is markedly increased. This is supported by Runt et al.,[30] who reported that the position of the Tα_2 can be influenced by the inclusion of single MDI and short MDI-BDO sequences into the soft phase. In agreement with the tensile modulus results, the storage modulus was observed to increase with the addition of 2 and 4 wt % organosilicates, indicating reinforcement has been provided to the TPU matrix. Somewhat incongruous values for the storage

dx.doi.org/10.1021/ma202189e | Macromolecules 2012, 45, 198–210

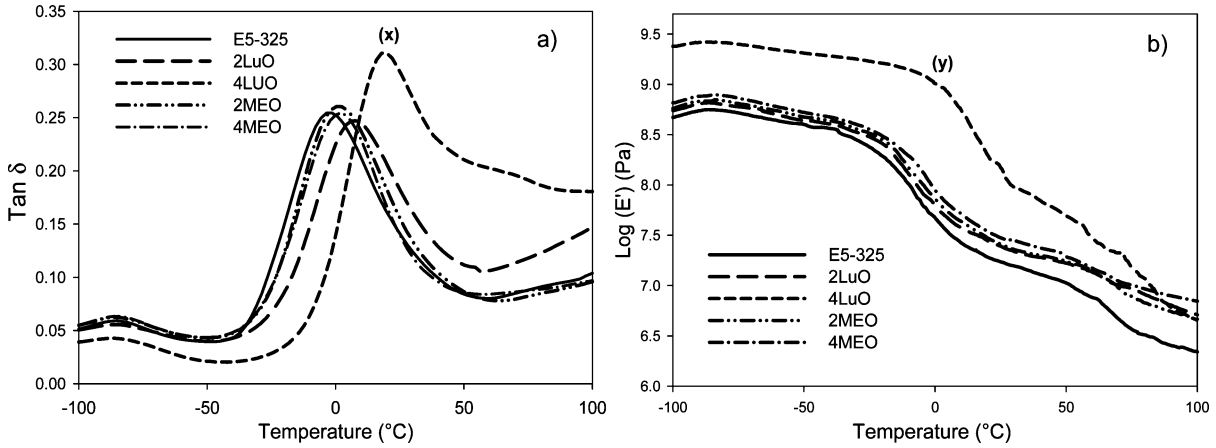

Figure 6. DMTA data as a function of temperature: (a) damping factor (tan δ); (b) storage modulus (E') for E5-325 (host TPU and nanocomposites). Curves (x) and (y) demonstrate that the 4LuO has a much higher soft microphase transition temperature (Tα_2) and storage modulus as compared to the neat host TPU, which indicates pronounced phase mixing.

Table 3. Transition Temperatures (α_1 and α_2) Determined from DMTA Curves

		damping peaks	
matrix	nanofiller	α_1 (°C)	α_2 (°C)
E5-325 TPU		−85.4	−3.0
	2LuO	−85.6	7.1
	4LuO	−86.3	18.0
	2MEO	−86.1	2.1
	4MEO	−84.2	2.0

modulus were observed for the 4 wt % LuO, nanocomposite system (Figure 6b). In agreement with mechanical test results, LuO was most effective in increasing the modulus of E5-325 at room temperature. However, these values are much higher in the glassy region but dropped drastically in the rubbery region (~50 °C). On the basis of this analysis, it was postulated that the addition of 2 wt % LuO in the TPU resulted in a "partial compatibilizing effect" while adding the organosilicate at 4 wt % induced almost full compatibilization between the hard and soft segments. The DSC and *in situ* SAXS data presented in the following section provide further supporting evidence for this phenomenon.

Differential Scanning Calorimetry (DSC). Table 4 summarizes the DSC features of the solvent-cast E5-325 (neat host TPU and nanocomposites) while Figures 7a and 7b present the heating and cooling thermograms, respectively. The enthalpy of fusion of hard segment melting endotherms is labeled as ΔH_m while the enthalpy of crystallization of hard segment is indicated by ΔH_c.

From the heating scan, we observed two to four endotherms in the DSC thermograms, and they have been labeled T1, T2, T3, and T4. Previous DSC analysis by Runt et al.[35] on similar PDMS-based TPU systems with PDMS/PHMO (in a ratio of 80/20) and 32.5% hard segment demonstrated an endotherm at ~50 °C and has been proposed to correspond to the ordering of single ("lone") MDIs.[35,36] A T2 endotherm was observable in the 99−115 °C range and is related to the T_g of the hard domains (T_{gH}) where the T_g of the high-molecular-weight hard segments (MDI-BDO) has been found to be around 110 °C.[37] In the case of 2LuO, a broader and more diffuse T2 peak suggests a more substantial paracrystalline interphase in this particular nanocomposite, compatibilized by the LuO organosilicate. At the same filler concentration, the LuO nanocomposites showed higher ΔH_m values when compared to the MEO nanocomposites. The ΔH_m values are highest for E5-325 containing 4LuO and lowest for E5-325 with 2MEO. In the 2LuO, a sharp hard segment melting endotherm (T3) centered at ~197 °C was observable and could be attributed to the nucleation or "self-assembly" of a higher melting hard microphase. In the case of 4LuO, the high-temperature melting endotherms (T3 and T4) were also appearing at temperatures of 194−207 °C. These high melting endotherms were perhaps due to sluggish, but preferential, organization of the longer hard segment present in this system at elevated temperatures. This is based on the previous DMTA analysis, where we have postulated that the 4LuO had

Table 4. Summary of DSC Heating and Cooling Curves of E5-325 (Neat Host TPU and Nanocomposites)

		heating					cooling	
		endotherm peak					crystallization exotherm	
matrix	nanofiller content	T1 (°C)	T2 (°C)	T3 (°C)	T4 (°C)	hard phase ΔH_m (J/g)[a,b]	peak (°C)	ΔH_c (J/g)[b]
E5-325 TPU		60	102			14.0	86	14.8
	2LuO	59	100	197		13.8	133	c
	4LuO	57	98	194	207	42.0	123	2.5
	2MEO	58	101			11.1	88	13.6
	4MEO	62	107			15.9	87	13.8

[a]Enthalpy of fusion values are the sum of the T1−T4 melting enthalpies. [b]Enthalpies were calculated per gram of hard segment (not per gram of sample). [c]Endotherm was too small to calculate an enthalpy value.

dx.doi.org/10.1021/ma202189e | *Macromolecules* 2012, 45, 198−210

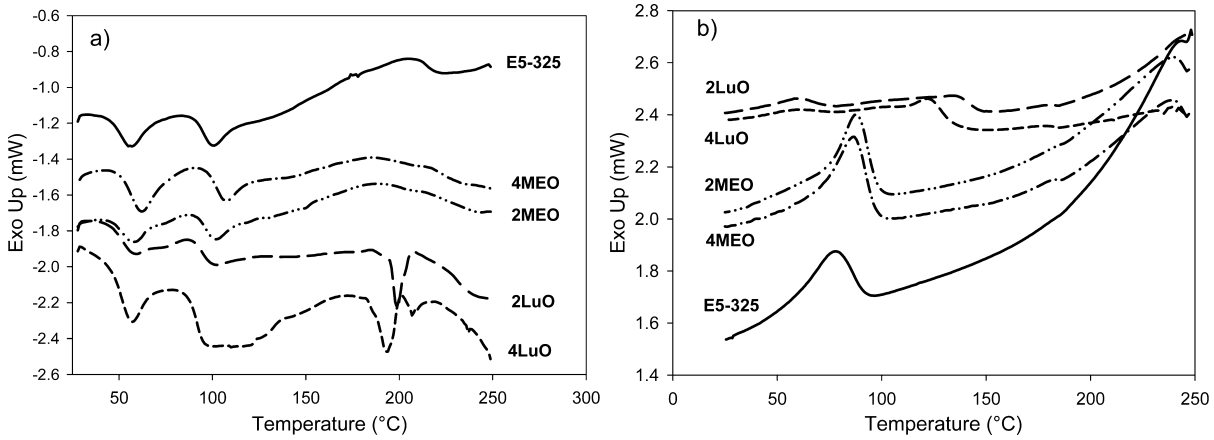

Figure 7. Typical DSC (a) heating curves and (b) cooling curves for the neat host TPU and containing LuO and MEO.

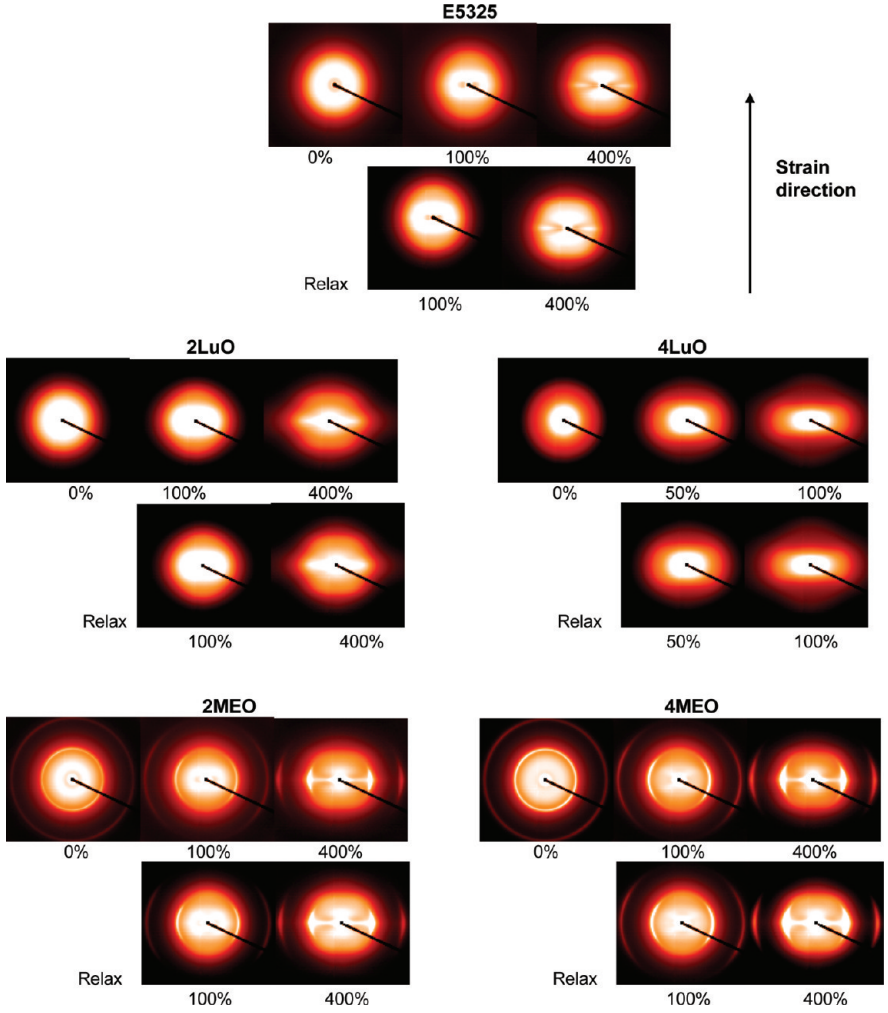

Figure 8. 2D SAXS patterns at selected strains for E5-325 (neat host TPU and nanocomposites) obtained from the short sample-to-detector distance. The relaxed state refers to images taken 10 min after strain measurements were taken.

compatibilized the hard and soft TPU segments. However, the longer hard segments are potentially excluded (insoluble) from the soft segments and interphases due to their thermodynamic incompatibility. Therefore, the high melting endotherms appear to relate to selective crystallization of the longer hard segment fractions that may be unable to dissolve in this phase-mixed system. As discussed previously, the anomalous tensile test and DMTA results obtained from these nanocomposite systems are attributed to these significant TPU morphological changes. Based on the cooling scan, crystallization exotherm peaks at 88 to 87 °C were observable for the E5-325 containing 2MEO and 4MEO, respectively. Meanwhile, for LuO nanocomposites, the crystallization exotherms were seen to occur at higher temperature which suggests that these lower aspect ratio organo-silicates provide a proportion of the TPU hard segments with a higher driving force to crystallize. However,

dx.doi.org/10.1021/ma202189e | *Macromolecules* 2012, 45, 198–210

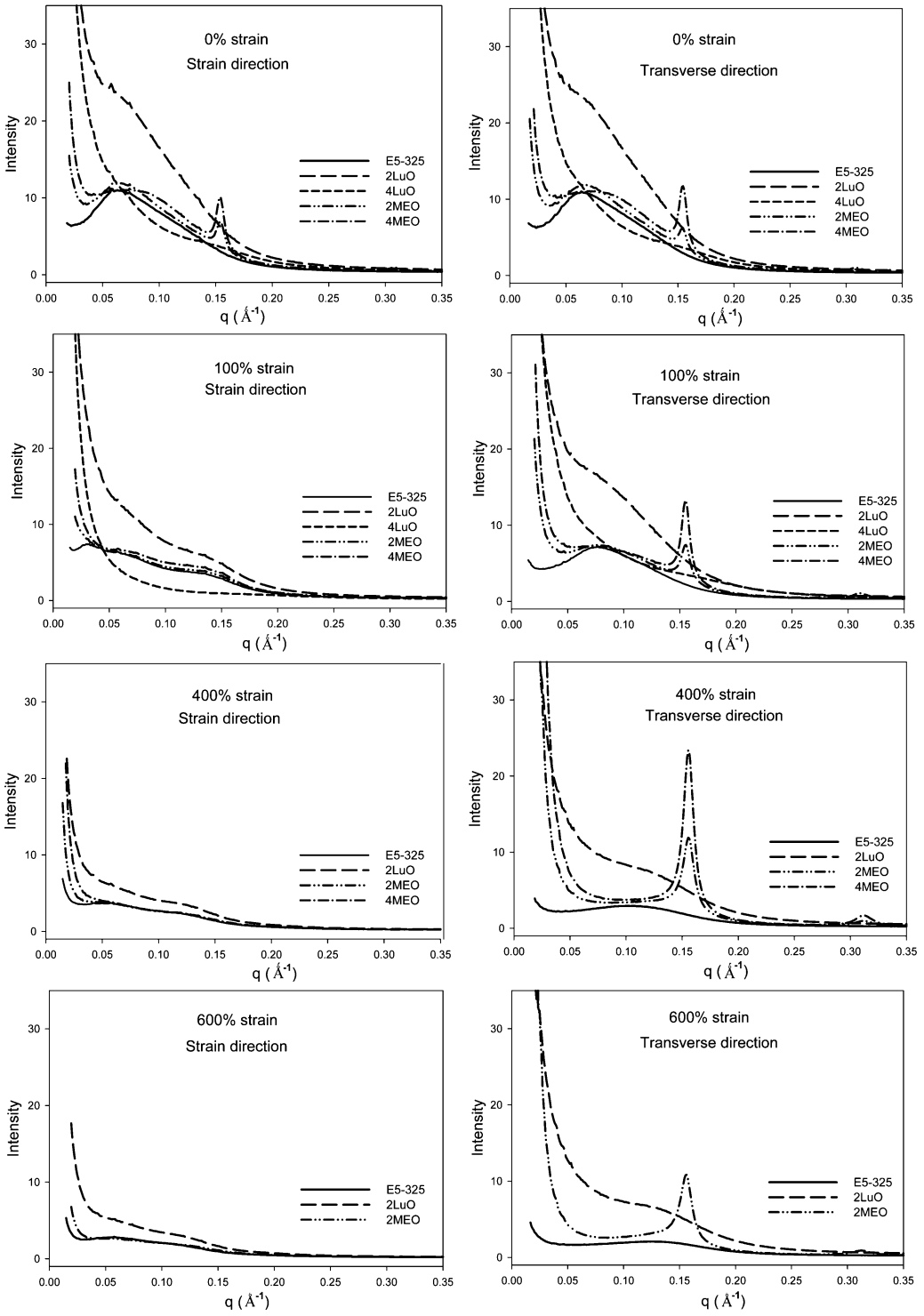

Figure 9. 1D profiles of E5-325, 2LuO, 4LuO, 2MEO, and 4MEO at 0%, 100%, 400%, and 600% strain in the strain and transverse direction, obtained from the short sample-to-detector distance.

they also exhibited lower ΔH_c values with a broader and weaker peak, which indicates that there is a disruption to the reorganization of complete population of hard segments during cooling from melt, perhaps brought about by the hydrophobic LuO simultaneously acting as both a nucleating and a compatibilizing agent.

***In Situ* Strained Small-Angle X-ray Scattering (SAXS).** Complete morphological characterization is vital to develop an in-depth understanding of structure−property relationships of the E5-325 TPU and associated nanocomposites. Static morphology and morphological evolution during stretching are both very important in these systems. *In situ* SAXS analysis of strained films is perhaps one of the most useful ways to probe structural changes.[19,38−40] The response of this microstructure to deformation facilitates an understanding of organosilicate orientation, TPU microdomain deformation, and associated cooperative toughening mechanisms. *In situ* SAXS under tensile deformation was therefore performed for all

dx.doi.org/10.1021/ma202189e | *Macromolecules* 2012, 45, 198−210

Table 5. Zernike Prins (ZP) Fits of SAXS Data of E5-325 (Neat Host TPU and Nanocomposites)

		strain direction			transverse direction		
strain (%)		d, nm (±0.5)[a]	R, nm (±0.5)	σ/d (±0.05)	d, nm (±0.5)	R, nm (±0.5)	σ/d (±0.05)
0	E5-325	9.5	2.7	0.32	9.4	2.7	0.22
	2LuO	9.8	2.7	0.57	9.7	2.7	0.35
	2MEO	8.3	2.7	0.43	8.2	2.7	0.44
	4MEO	6.8	2.6	0.51	6.8	2.6	0.51
50	E5-325	11.4	2.8	0.35	8.7	2.7	0.61
	2LuO	10.1	2.9	0.42	8.7	2.7	0.89
	2MEO	9.0	2.8	0.21	7.9	2.7	0.59
	4MEO	7.6	2.6	0.58	6.7	2.5	0.56
100	E5-325	16.9	2.7	0.62	8.2	2.7	0.60
	2LuO	10.7	3.0	0.37	7.9	2.7	0.50
	2MEO	7.4	2.7	0.23	7.2	2.5	0.77
	4MEO	7.7	2.6	0.38	6.4	2.3	0.90
200	E5-325	7.5	2.7	0.74	7.5	2.6	0.61
	2LuO	9.8	2.9	0.44	6.0	2.7	0.94
	2MEO	7.5	2.7	0.64	6.3	2.2	0.77
	4MEO	7.1	2.6	0.35			
400	E5-325	8.5	2.6	0.50	6.5	2.5	0.60
	2LuO				5.3	2.5	0.85
	2MEO	7.8	2.7	0.81			
	4MEO	10.8	2.6	0.42			
600	E5-325	8.6	2.6	0.91	5.9	2.5	0.53
	2LuO				5.2	2.5	0.74
	2MEO	7.3	2.4	0.93			
	4MEO[b]						

[a]Expected uncertainty due to sample variations and curve fitting. [b]Sample broke.

samples, in an effort to better elucidate the mechanisms responsible for the mechanical behaviors observed. The scattered radiation achieves higher intensity levels when organo-silicates are incorporated into TPU due to their very high electron scattering length density with respect to TPU segments. Therefore, analysis at different q regions was done in order to differentiate between TPU morphology and contributions from the nanofillers. The SAXS data obtained at the short sample-to-detector distance (q range of 0.015−0.50 Å) was used to study changes in TPU microphase morphology, while the data collected at the long sample-to-detector distance (q range of 0.002−0.06 Å) was used to follow the evolution of nanosilicate morphology during uniaxial loading.

TPU Microphase Morphology during Deformation. 2D SAXS images at selected strains for the neat host TPU and nanocomposites collected at the short sample-to-detector distance during deformation are shown in Figure 8, together with the images acquired after relaxing the stretched films for 10 min. Their respective 1D SAXS profiles are shown in Figure 9.

In the initial unstrained state, all samples show isotropic SAXS patterns, indicating that the hard segment domains are randomly oriented, which then transforms to increasingly anisotropic patterns upon stretching. The neat E5-325 exhibits a typical TPU SAXS pattern.[19,32,41,42] At 100% strain, the ring deforms to an ellipsoid with the long axis along the equator. The *in situ* SAXS studies of TPU containing 42 wt % hard segment by Blundell et al.[41] showed that the elliptical SAXS pattern is attributed to an affine deformation of the two-phase structure of TPU, similar to the findings of Desper and co-workers.[42] It is reasonable to assume that the soft segments are mainly involved in the deformation of this material during the first 100% strain, and the TPU hard segments respond to the alignment of the soft segment chains at this stage. The SAXS pattern reveals scattering lobes on the meridian and a streak in the equatorial direction when the strain reaches 400%. This scattering pattern is an indicative of a certain degree of orientation of the hard segments and the existence of oriented soft segment microphases, all of which are aligning in the stretch direction. The equatorial streak appears as a result of reduced electron density contrast between the hard segment nanofibrils and the aligned soft segment chains and/or the decrease in coherent scattering due to the small size of the broken down hard domains. This effect can be observed from the reduction of the average hard domain spacing (Table 5) when the strain reaches and surpasses 200%.

At low elongation (100%), the 2D SAXS pattern of 2LuO is similar to the neat TPU, showing an ellipse scattering. However, upon straining to 400%, the equatorial scattering appears wider with respect to that observed in other materials, suggesting the presence of longer, more fragmented hard segment domains. The SAXS pattern of 4LuO, due to strong phase mixing, exhibits plastic behavior rather than elastomeric deformation as the system was tested about its T_g. The sample broke at 125% strain. Conversely, the SAXS patterns for MEO nanocomposites demonstrate an isotropic outer ring prior to straining, which then progressively transforms into two arcs in the equator upon straining. This outer ring is located in the high q region, relates to the diffraction from registered high aspect ratio fluoromica tactoids, and is understandably more intense in the material containing a higher organo-fluoromica loading (4MEO). At 100% strain, the two arcs observed in the region of q = 0.15−0.17 Å^{-1} represent the oriented nanoparticles, and the respective scattering peak at q = 0.155 Å^{-1} can be observed in the SAXS profile (Figure 9). At 400% strain, the

dx.doi.org/10.1021/ma202189e | *Macromolecules* 2012, 45, 198−210

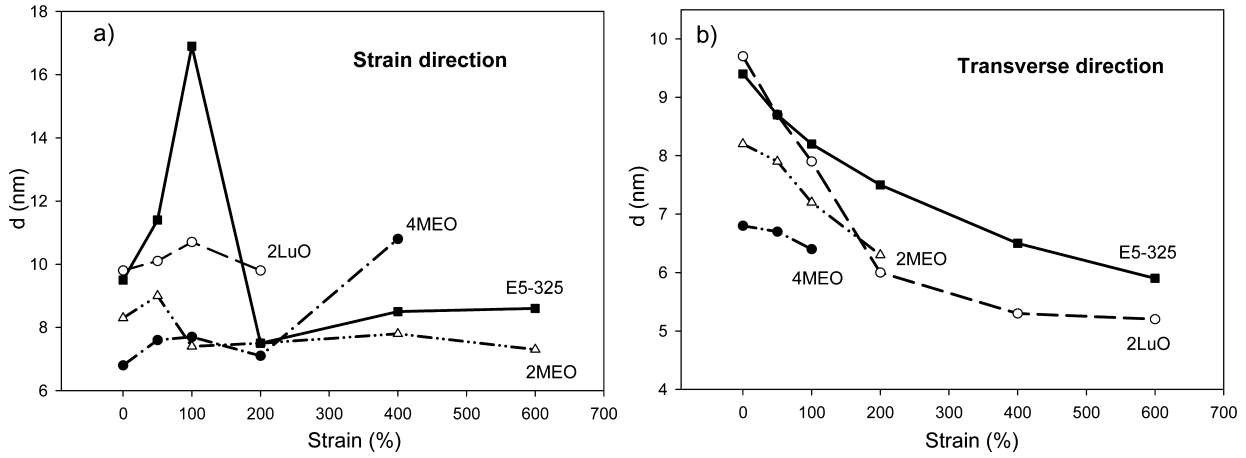

Figure 10. Estimated average hard domain spacing (d) of the neat host TPU and nanocomposites determined from the Zernike−Prins model in the (a) strain and (b) transverse direction.

arcs become broader, which suggests that a higher fraction of nanoparticles become oriented in the strain direction.

For all strained samples, slightly intensified scattering was observable from SAXS patterns during the relaxation process, indicating a slight recovery of phase separation and hard segment ordering. However, the nanocomposite samples show a lesser degree of recovery due to reduced TPU microphase mobility as a result of organosilicate inclusion.

The 1D SAXS profiles presented in Figure 9 of the neat host TPU and nanocomposites reveal prominent peaks in the region of q = 0.06−0.09 Å^{-1}, corresponding to the segmental microphase periodicity in the materials. Further stretching results in the decrease in the scattering intensity, in both strain and transverse directions, which suggests a disruption of the hard segment domain fraction.[43] Another two reflections (q = 0.155 and q = 0.31 Å^{-1}), corresponding to diffraction from the fluoromica tactoids with d-spacing of 4.2 and 2.1 nm, respectively, were observable in the undeformed 2MEO and 4MEO samples. Both scattering peaks appear stronger and shift slightly toward higher q in the transverse direction as the strain increases from 0% to 600%, suggesting greater organosilicate alignment and reduced spacing between the individual platelets. The XRD analysis on the undeformed 2MEO and 4MEO as shown in Figure 2b also confirms the presence of a similar organo-silicate d-spacing.

Based on Figures 8 and 9, there are clear differences in periodicity and in the degree of order between the LuO and MEO nanocomposite systems. Other than a broader peak, 2LuO demonstrates much higher scattering intensity in the q region between 0.02 and 0.15 Å^{-1}, even after silicate subtraction. Although the LuO organosilicate is believed to induce some degree of phase mixing in the system, there is also strong evidence from the DSC thermograms for the nucleation of "self-assembly" of a higher melting (T_m) hard microphase. We believe that a population of longer hard segments and LuO platelets may be cooperating to form a restructured hard domain. The high-intensity scattering observed might be due to the better contrast of this more well-ordered hard segment population. The intensity curves of the 4LuO decrease monotonically without a diffraction maximum. This featureless SAXS pattern implies the strong phase mixing between the hard and soft segments in this TPU nanocomposite system. Similarly, no significant scattering from the organo-silicate was detected in the XRD analysis.

The change in hard domain spacing (d) with deformation for E5-325 TPU and nanocomposites was also studied from the SAXS patterns. The morphological data obtained from the ZP fitting, combined with the direct visualization of the 1D scattering profiles, are tabulated in Table 5 and presented graphically in Figure 10.

For the neat host TPU, the d-spacing is observed to increase sharply in the strain direction at the initial stages of deformation. The randomly oriented hard domains subjected to tensile deformation exhibited an increase of d-spacing from 9.5 to 16.9 nm upon 100% strain. In relation to affine deformation, it is reasonable to assume that the TPU hard blocks respond to the alignment of the soft segment chains at this stage. Subsequent deformation up to 200% strain resulted in a decrease in the d-spacing to 7.5 nm, as the hard segment aggregates are disrupted, broken down to smaller widths, and partially aligned in the direction of stretch. Further stretching gives no significant effect to the d-spacing of the neat TPU. Conversely, straining the TPU nanocomposites up to 200% is associated with only slight shifts of d in the strain direction, most notably seen in the 2LuO system. On the basis of TEM images, 2LuO demonstrates greater organo-silicate dispersion and exfoliation in the TPU compared to the other nanocomposites, showing more individual organo-silicate layers available for molecular interaction with the TPU segments. This should result in higher restriction in mobility of the segment chains. In addition, the DSC, tensile creep, and stress relaxation studies also suggest the presence of additional hard domain connectivity in this system, which could lead to a better retention of hard domain spacing upon deformation. The ZP model was unable to fit the scattering data of high strained 2LuO in strain direction because the scattering peak had diminished. 2 wt % MEO at 100% resulted in the decrease of d, which could be due to rotation, reorganization, and tilting of the hard domains, perhaps induced by their interaction with the high aspect ratio platelets. Further stretching gives no significant effect to the interdomain spacing of this material. For all samples, a decrease in d is observed in the transverse direction with increasing strain. This is expected as the system was subjected to uniaxial deformation. As compared to other systems, 2LuO, which contains more cohesive hard microdomains, presents a significant reduction of d in the transverse direction, possibly due to the deformed hard domain and better preferred orientation of LuO with straining. The ZP model was

dx.doi.org/10.1021/ma202189e | Macromolecules 2012, 45, 198−210

unable to fit the scattering data of high strained MEO nanocomposites in the transverse direction because the scattering peak had diminished. In all cases, the hard segment radius of gyration (R) did not change significantly over the entire strain range. The data fitting was more sensitive to the position of the peak in the scattering profile, and hence the d value, than to the form factor contribution, and hence the R value.

Organo-silicate Orientation during Tensile Deformation. The orientation of the organo-silicate during uniaxial deformation plays an important role in the toughness enhancement of the TPU.[19,44] The scattering profiles obtained from the deformation process provide very useful insights into morphological changes in the nanostructure during strain. Figure 11 displays the selected 2D SAXS patterns of the neat

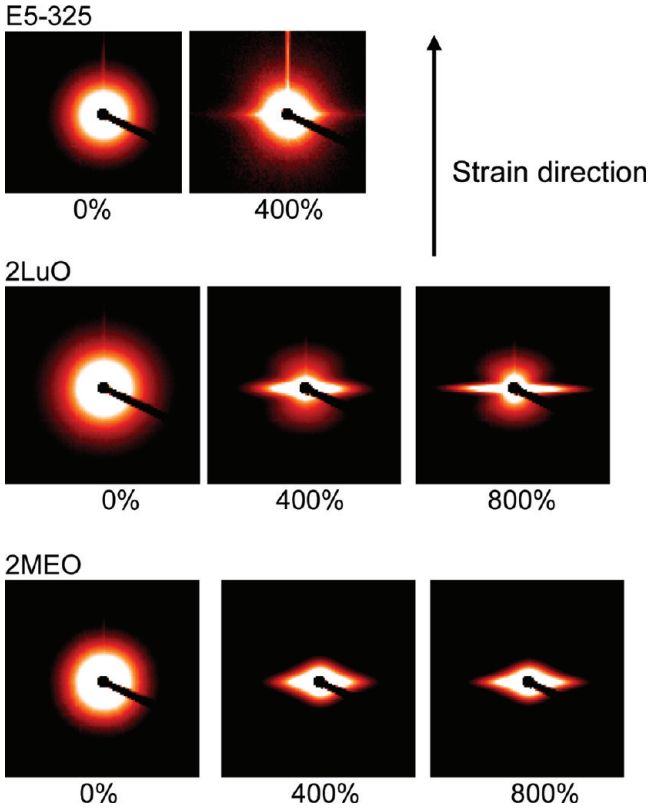

Figure 11. Selected 2D SAXS patterns at various strains for E5-325, 2LuO- and 2MEO, obtained from the long sample-to-detector distance.

host TPU and nanocomposites, obtained from the long sample-to-detector distance.

For the neat TPU, the absence of organo-silicate led to the isotropic SAXS patterns during unstrain and 400% strain. Note that the sample broke before reaching 800% strain. Meanwhile for the nanocomposites, the initially isotropic SAXS patterns were found to become anisotropic as the strain was increased. For 2LuO, the meridian stripe was seen to develop at 400% strain, which then become increasingly sharper toward the transverse direction when the strain reached 800%. This is indicative of significant platelet alignment in the strain direction. In comparison, the MEO nanocomposites demonstrate different scattering geometry. A diamond-shaped pattern suggests that there was alignment of fluoromica tactoids in both the strain and transverse direction, presumably due to delamination of matrix and nanofiller in some instances and effective load transfer and tactoid orientation in others.[19] The Herman orientation function (f) was calculated at q = 0.0031, where the scattering is dominated by the nanosilicates. These values are illustrated in Figure 12.

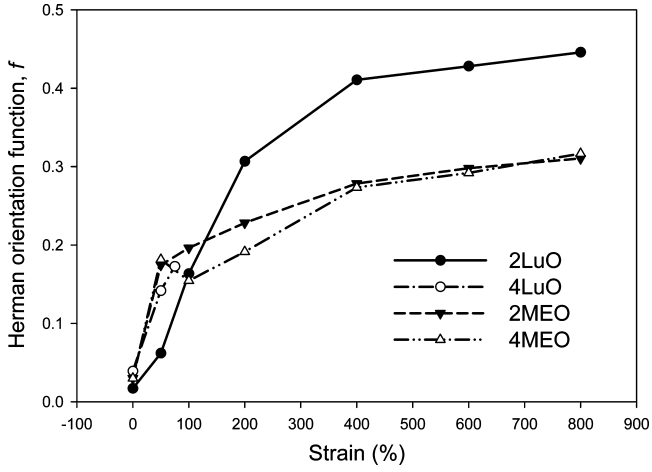

Figure 12. Herman orientation function versus strains for E5-325 TPU nanocomposites.

In the initial stages of deformation, the preferred orientation and alignment of high aspect ratio MEO nanocomposites are due to casting and settling during solvent casting. However, the degree of platelets alignment at high strains (>200%) was significantly greater for 2LuO than for 2MEO and 4MEO nanocomposites. This suggests that the low aspect ratio LuO aligns more preferentially in the strain direction than the high aspect ratio MEO at similar concentration during uniaxial tension of TPU, which is similar to the findings reported by Finnigan et al.[19] Large tactoids present in 2MEO and 4MEO are less mobile and having lower capability to align in the strain direction. Tactoids and unaligned platelets led to the formation of voids due to developed tensile stresses at the interface between the tactoids and the TPU. This can be visualized from the stress whitening effect developed in both 2MEO and 4MEO sample upon straining (figure not shown). This explains why the presence of 2LuO in the TPU leading to greater improvement in toughness compared to the 2MEO. As expected, the lower concentration of MEO (2 wt %) was found to be more aligned than the higher concentration MEO (4 wt %) in the TPU matrix.

■ SUMMARY

In summary, both high and low aspect ratio organosilicates resulted in broadly enhanced mechanical properties of this PDMS-based TPU system when added at 2 wt %. The low aspect ratio organosilicate when added in 2 wt % was seen to disperse and delaminate well in the TPU matrix, providing additional hard domain connectivity and brought about appreciable enhancements in tensile and tear strength and also markedly improved creep resistance. However, in the case of higher filler loadings (4 wt %), the hydrophobic low aspect ratio organosilicates induced profound morphological changes in the TPU microdomain texture, thus adversely effecting the mechanical properties of the E5-325 TPU. This can be seen from a dramatic increase in soft microphase transition temperature and profound stiffening effect. Thus, it is proposed

dx.doi.org/10.1021/ma202189e | Macromolecules 2012, 45, 198–210

that the hydrophobic low aspect ratio organosilicate acts as a very potent interfacial compatibilizer, which can effectively alter the morphological response of the TPU to deformation but needs to be introduced carefully in order to exploit its full utility.

AUTHOR INFORMATION

Corresponding Author

*E-mail: darren.martin@uq.edu.au.

ACKNOWLEDGMENTS

The authors thank Aortech Biomaterials Pty Ltd. and Cochlear Ltd. for research materials and financial support. This work was carried out in part on the SAXS/WAXS beamline at the Australian Synchrotron, Victoria, Australia. We also appreciate the facilities as well as the scientific and technical assistance of the Centre for Microscopy and Microanalysis, University of Queensland, and personally to Dr. Garry Morgan for the expert F30 training he provided. Azlin F. Osman expresses her appreciation to the Ministry of Higher Education Malaysia and University Malaysia Perlis for financial support. Finally, we also thank Prof. James Runt (Penn State University) and Dr. Nigel Kirby (Australian Synchrotron) for much time and effort adapting our tensometer for the Australian Synchrotron.

REFERENCES

(1) Anderson, J.; Hiltner, A.; Wiggins, M.; Schubert, M.; Collier, T.; Kao, W.; Mathur, A. *Polym. Int.* **1999**, *46*, 163−171.

(2) Pinchuk, L. *J. Biomater. Sci., Polym. Ed.* **1995**, *6*, 225−267.

(3) Szycher, M.; McArthur, W. In *Surface Fissuring of Polyurethanes Following in Vivo Exposure*; ASTM International: West Conshohocken, PA, 1985; p 308.

(4) Lelah, M.; Cooper, S. *Polyurethanes in Medicine;* CRC Press, Inc.: Boca Raton, FL, 1986; p 225.

(5) Szycher, M. *J. Biomater. Appl.* **1988**, *3*, 297.

(6) McCarthy, S.; Meijs, G.; Mitchell, N.; Gunatillake, P.; Heath, G.; Brandwood, A.; Schindhelm, K. *Biomaterials* **1997**, *18*, 1387−1409.

(7) Williams, D. F. *Progress in Biomedical Engineering*; Elsevier: Amsterdam, 1987.

(8) Gunatillake, P.; Meijs, G.; Mccarthy, S.; Adhikari, R. *J. Appl. Polym. Sci.* **2000**, *76*, 2026−2040.

(9) http://www.aortech.com/technology/elast-eon.

(10) Mishra, A.; Nando, G.; Chattopadhyay, S. *J. Polym. Sci., Part B: Polym. Phys.* **2008**, *46*, 2341−2354.

(11) Mishra, A.; Chattopadhyay, S.; Nando, G. *J. Appl. Polym. Sci.* **2010**, *115*, 558−569.

(12) Korley, L. S. T. J.; Liff, S. M.; Kumar, N.; McKinley, G. H.; Hammond, P. T. *Macromolecules* **2006**, *39*, 7030−7036.

(13) Kim, W.; Chung, D.; Kim, J. *J. Appl. Polym. Sci.* **2008**, *110*, 3209−3216.

(14) Barick, A. K.; Tripathy, D. K. *J. Appl. Polym. Sci.* **2010**, *117*, 639−654.

(15) Smart, S.; Fania, D.; Milev, A.; Kannangara, G.; Lu, M.; Martin, D. *J. Appl. Polym. Sci.* **2010**, *117*, 24−32.

(16) Campbell, K. T. The Structure of Segmented Polyurethane Nanocomposites. PhD Thesis, University of Queensland, 2005.

(17) Martin, D.; Edwards, G. Polymer Composites Having Particles with Mixed Organic Modifications. 15 April, 2009.

(18) Laity, P. R.; Taylor, J. E.; Wong, S. S.; Khunkamchoo, P.; Norris, K.; Cable, M.; Andrews, G. T.; Johnson, A. F.; Cameron, R. E. *Polymer* **2004**, *45*, 7273−7291.

(19) Finnigan, B.; Jack, K.; Campbell, K.; Halley, P.; Truss, R.; Casey, P.; Cookson, D.; King, S.; Martin, D. *Macromolecules* **2005**, *38*, 7386−7396.

(20) Pethrick, R. A.; Dawkins, J. *Modern Techniques for Polymer Characterisation*; J. Wiley: New York, 1999.

(21) Roe, R. J.; Roe, R. *Methods of X-ray and Neutron Scattering in Polymer Science*; Oxford University Press: New York, 2000.

(22) Malwitz, M. M.; Lin Gibson, S.; Hobbie, E. K.; Butler, P. D.; Schmidt, G. *J. Polym. Sci., Part B: Polym. Phys.* **2003**, *41*, 3237−3248.

(23) Pinnavaia, T.; Lan, T.; Wang, Z.; Shi, H.; Kaviratna, P. In *Clay-Reinforced Epoxy Nanocomposites: Synthesis, Properties, and Mechanism of Formation*; ACS Publications: Washington, DC, 1996; pp 250−261.

(24) Alexandre, M.; Dubois, P. *Mater. Sci. Eng., R* **2000**, *28*, 1−63.

(25) Chen, C.; Mao, C.; Tsai, M.; Yen, F.; Lin, J.; Tseng, C.; Chen, H. *J. Appl. Polym. Sci.* **2008**, *110*, 237−243.

(26) Finnigan, B.; Martin, D.; Halley, P.; Truss, R.; Campbell, K. *J. Appl. Polym. Sci.* **2005**, *97*, 300−309.

(27) Breu, J.; Seidl, W.; Stoll, A.; Lange, K.; Probst, T. *Chem. Mater.* **2001**, *13*, 4213−4220.

(28) Yang, J.; Han, Y.; Choy, J.; Tateyama, H. *J. Mater. Chem.* **2001**, *11*, 1305−1312.

(29) Choi, T.; Weksler, J.; Padsalgikar, A.; Runt, J. *Polymer* **2009**, *50*, 2320−2327.

(30) Hernandez, R.; Weksler, J.; Padsalgikar, A.; Runt, J. *Macromolecules* **2007**, *40*, 5441−5449.

(31) Liff, S.; Kumar, N.; McKinley, G. *Nature Mater.* **2007**, *6*, 76.

(32) Yeh, F.; Hsiao, B.; Sauer, B.; Michel, S.; Siesler, H. *Macromolecules* **2003**, *36*, 1940−1954.

(33) Wang, Z.; Pinnavaia, T. *Chem. Mater.* **1998**, *10*, 3769−3771.

(34) Sternstein, S.; Zhu, A. J. *Macromolecules* **2002**, *35*, 7262−7273.

(35) Hernandez, R.; Weksler, J.; Padsalgikar, A.; Choi, T.; Angelo, E.; Lin, J.; Xu, L.; Siedlecki, C.; Runt, J. *Macromolecules* **2008**, *41*, 9767−9776.

(36) Martin, D.; Meijs, G.; Renwick, G.; Mccarthy, S.; Gunatillake, P. *J. Appl. Polym. Sci.* **1996**, *62*, 1377−1386.

(37) Pongkitwitoon, S.; Hernández, R.; Weksler, J.; Padsalgikar, A.; Choi, T.; Runt, J. *Polymer* **2009**, *50*, 6305−6311.

(38) Yeh, F.; Hsiao, B. S.; Sauer, B. B.; Michel, S.; Siesler, H. W. *Macromolecules* **2003**, *36*, 1940−1954.

(39) Christenson, E. M.; Anderson, J. M.; Hiltner, A.; Baer, E. *Polymer* **2005**, *46*, 11744−11754.

(40) Koerner, H.; Kelley, J. J.; Vaia, R. A. *Macromolecules* **2008**, *41*, 4709−4716.

(41) Blundell, D. J.; Eeckhaut, G.; Fuller, W.; Mahendrasingam, A.; Martin, C. *Polymer* **2002**, *43*, 5197−5207.

(42) Desper, C.; Schneider, N.; Jasinski, J.; Lin, J. *Macromolecules* **1985**, *18*, 2755−2761.

(43) Fu, B.; Hsiao, B.; Pagola, S.; Stephens, P.; White, H.; Rafailovich, M.; Sokolov, J.; Mather, P.; Jeon, H.; Phillips, S. *Polymer* **2001**, *42*, 599−611.

(44) Shah, D.; Maiti, P.; Jiang, D. D.; Batt, C. A.; Giannelis, E. P. *Adv. Mater.* **2005**, *17*, 525−528.